

Introducing Series Elastic Links for Affordable Torque-Controlled Robots

Andrea Calanca , Eldison Dimo , Rudy Vicario , Paolo Fiorini , Mauro Serpelloni, and Giovanni Legnani

Abstract—Robotics has the potential to become a revolutionary technology in the next future and if we want to spread it among the population we must start accounting for affordability in robot research and design. Plastic robots are an emerging example of affordable design where expensive metal structures are replaced by low-cost plastic materials. Plastic materials are not only cost effective but, thanks to their inherent compliance and lightweight, lead to significant advantages in terms of safety and force controllability. Inspired by the idea of series elastic actuator (SEA) this letter introduces the new concept of series elastic link (SEL), which exploits the inherent flexibility of plastic links to implement series compliance. This letter elaborates on the concept of SEL and highlights a parallelism with SEAs. Then, focusing on a single-DOF setup it shows that, beyond their economic advantage, SELs lead to enhanced safety and more accurate force control with respect to traditional SEA implementations. The proposed argumentations are theoretically supported and experimentally validated.

Index Terms—Series elastic links, series elastic actuators, force control, physical human-robot interaction, consumer robotics.

I. BACKGROUND

THE use of robotics in contemporary society is rapidly increasing. While rehabilitation robots are today used in big and medium therapeutic centers to more efficiently deliver physical treatments, the Cybathlon competition is promoting the development of assistive robotics for disabled people which is expected to allow independence in their daily activities. Even if the price of robots is continuously decreasing thanks to scale economies, further steps are required to target the available income of the majority of population and to meet widespread human needs. Up to now, few research efforts are spent to investigate design paradigms that can guarantee both affordability and human-oriented capabilities, i.e., the capabilities to cope, support and interact with humans in a natural and safe way. Human-oriented robots are expected to sense the physical interaction with humans and to quickly react using force control

Manuscript received June 15, 2018; accepted September 27, 2018. Date of publication October 26, 2018; date of current version December 6, 2018. This letter was recommended for publication by Associate Editor Q. Xu and Editor D. Popa upon evaluation of the reviewers' comments. This work was supported by the project of the Italian Ministry of Education, Universities and Research (MIUR) "Dipartimenti di Eccellenza 2018-2022." (Corresponding author: Andrea Calanca.)

A. Calanca, E. Dimo, R. Vicario, and P. Fiorini are with the Department of Computer Science, University of Verona, Verona 37134, Italy (e-mail: andrea.calanca@gmail.com; eldison.dimo@studenti.univr.it; rudy.vicario@studenti.univr.it; paolo.fiorini@univr.it).

M. Serpelloni and G. Legnani are with the Department of Information Engineering and Mechanical Engineering, University of Brescia, Brescia 25123, Italy (e-mail: mauro.serpelloni@unibs.it; giovanni.legnani@unibs.it).

Digital Object Identifier 10.1109/LRA.2018.2878353

technology [1], [2]. Also, to collaborate with humans and to support their functions, these robots are expected to exert relatively high forces (within the human range) with a high level of safety. Unfortunately, at the current state of the technology only high-cost robotic systems can provide these capabilities [3]–[5].

This letter proposes a fundamental building block in the direction of designing affordable torque-controlled robots. Based on the assumption that in different robotic applications plastic materials will substitute metal structures, we introduce the concept of Series Elastic Link (SEL) which exploits the inherent flexibility of plastic links to implement compliant actuation and control using inexpensive components. Compliant actuators are a widespread technology to implement interaction control with a high level of stability robustness and transparency [2], [6], [7]. They are usually composed of a motor in series with a compliant element which is then connected to the robotic link. Unfortunately, even if it was proclaimed that such design enables "excellent force control out of inexpensive components" [8], in reality, several expensive spring design have been proposed in the literature to realize compact elastic actuators [9], [10]. The concept of SEL introduces an alternative compliance implementation: why adding expensive compliance in series with the actuator when the link itself can be compliant? The SEL design substitutes two high-cost components - the series spring and the rigid link - with a single inexpensive and lightweight compliant link which *becomes the force sensor*.

Flexible link robots have been widely discussed in the literature. In the past, link compliance was merely seen as a side effect of certain lightweight designs where the end-effector position needs to be accurately controlled in spite of undesired oscillations and inaccuracies due to the elastic dynamics [11], [12]. Differently, this letter considers a different application, interaction control, where link compliance is seen as an advantage rather than a side effect. Similarly to Series Elastic Actuators (SEAs) [6], the concept of SEL introduces the perspective of taking advantage of compliance rather than counteracting it. The idea of exploiting link compliance in interaction control applications has been rarely explored in the literature. The work by Malzahn represents one of the few significant examples. Given that the derivation and exploitation of a multi-elastic-body model is extremely complex and computationally intensive, one of the contribution of Malzahn has been to exploit decentralized control strategies to waive the need for a complex coupled elastic model [13]–[15]. Generally speaking, the high complexity of multi-elastic-body models make it extremely "difficult to apply theoretical closed-loop control strategies, which need

closed-form manipulations” of the complex beam dynamics; indeed, “varying joint configurations, unpredictable payload changes or physical contacts with the environment alter the boundary conditions to the governing beam partial differential equations” [12], [16]. As a consequence, existing investigations are often limited to simulation studies and single-DOF experiments [17], [18].

Up to now this amount of complexity hindered the diffusion of link compliance in favor of joint compliance which can be more easily modeled. Even in the approach by Malzahn, where decentralized inner controllers allow to approximate the system to a rigid-body dynamics, it is not clear how to deal with orientation errors given by link bending. Considering this background, this letter proposes a perspective change regarding single-DOF applications. Indeed, we argue that most of complexity in elastic link modeling arises only in the case of multi-DOF systems. Thus, we consider applications such as exoskeletons and single joint orthoses where the main objective is to deliver a specific torque profile at a specific joint. In these applications each robot joint maps a human joint and each robot link is attached to a human segment, thus, *the human is in direct contact with each robot link*. This letter shows that in such single-DOF applications joint compliance and link compliance can be modeled similarly and that SELs lead to possible advantages with respect to SEAs. Indeed, lightweight plastic links allows not only to reduce the cost but also to improve safety and impact tolerance and to more accurately estimate forces acting on the link. The letter is organized as follows: Section II reports a model for the SEL architecture considering links made of lightweight plastic tubes, Section III expands on the similarities between SELs and SEAs and motivates some advantages of SELs in single-DOF applications, Section V reports the experimental validation of our statements and Section VI reports our conclusions.

II. SERIES ELASTIC LINK MODELING

SEA and SEL architectures represent alternative implementations of the same concept: series compliance. Indeed, in this section we show that they can be modeled similarly: for small deflections the link bending stiffness can be translated into an equivalent joint torsional stiffness. Within the SEA literature, an established model for series compliance is the one represented in Fig. 1(a) where θ is the motor position, q is the environment position, τ_m is the motor input torque (proportional to the current), τ_s is the spring torque and τ_e represents the environment forces. The actuator parameters are the spring stiffness k and the reflected motor-gear inertia J_m . For simplicity of representation Fig. 1(a) translates angular variables (angles and torques) into linear equivalents (linear positions and forces), nevertheless the models in this letter refer to angular quantities. The model in Fig. 1(a) can be written as

$$J_m \ddot{\theta} = \tau_m - \tau_s \quad (1)$$

$$\tau_s = k(\theta - q) \quad (2)$$

where τ_s is the spring torque and we have $\tau_e = \tau_s$. However, when considering a robotic application driven by a SEA, this model can only represent the elastic actuator subsystem whereas

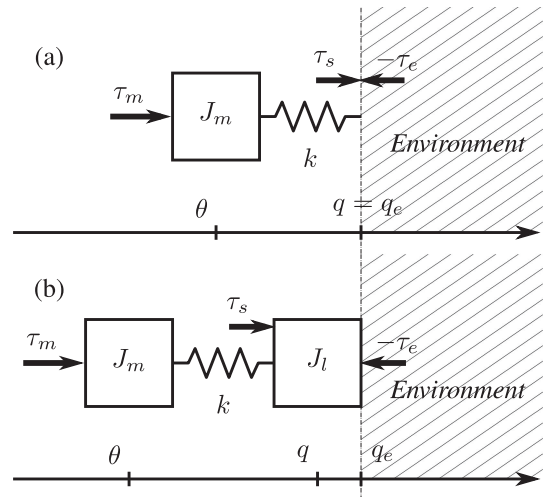


Fig. 1. (a) A wide used model for series compliance. In the case of SEA this model is quite unrealistic because it neglects the link inertia. In the case of SEL the link inertia is necessarily small and the same model becomes realistic. (b) A realistic model for SEA which includes the link inertia.

a more meaningful model should at least account for the dynamics of the link, as represented in Fig. 1(b). Here, more realistically, the SEA is in contact with the environment through the link. Indeed, the interaction with the environment necessarily involves the link which represents the physical robot-environment interface. The model in Fig. 1(b) can be expressed as

$$J_m \ddot{\theta} = \tau_m - \tau_s \quad (3)$$

$$J_l \ddot{q} = \tau_s - \tau_e \quad (4)$$

where J_l represents the link inertia. Consequently, in dynamical conditions the spring torque τ_s is different from the interaction torque τ_e because of the in-between link dynamics. Thus, τ_s - which is often used as a feedback signal [6], [7] - only provides an *indirect measure* of τ_e which is the true interaction force with the environment. Another side effect of the link inertia in model (4) is that a high link inertia may imply high impact forces during collisions with the environment, thus limiting system safety. Interestingly, given the lightweight of plastic materials, the SEL concept can alleviate these limitations. This will be theoretically supported in the next section. Here we show that SEL can be modeled similarly to model (1)–(2), i.e., as a SEA with negligible link inertia. To this aim we base on a couple of modeling assumptions that are detailed in the following.

The first modeling assumption regards sufficiently small link deflections. This allows to model the elastic link as a cantilever beam and to relate the link bending stiffness to an equivalent torsional stiffness k_{eq} . The considered cantilever beam model is represented in Fig. 2(a) where L is the beam length and Δx represents the end point displacement due to a perpendicular perturbing force F_e applied on the link endpoint. For small deflections the cantilever beam model leads to the following relation

$$\Delta x = -\frac{L^3}{3IE} F_e \quad (5)$$

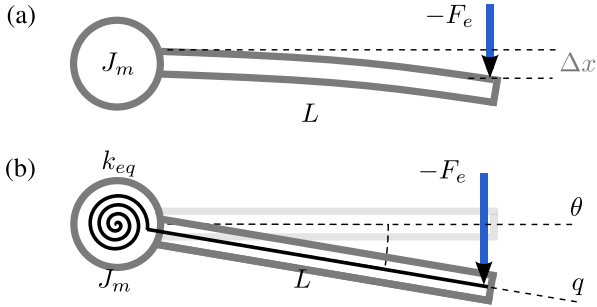


Fig. 2. (a) A flexible robot link modeled as a cantilever beam and deformed by a force F_e applied on the link endpoint. (b) An equivalent model for the link where the link deformation is expressed in terms of an equivalent torsional stiffness k_{eq} .

where E is the Young modulus of the beam material and I represents the area moment of inertia of the beam section. By considering again small deflections, translating linear quantities into angular equivalents, i.e., $\Delta x = L(\theta - q)$, and considering the force F_e as exerted by the environment, which generates the torque $\tau_e = LF_e$, the following equality can be computed

$$\tau_e = \frac{3IE}{L}(\theta - q) = k_{eq}(\theta - q) \quad (6)$$

which states that the equivalent stiffness k_{eq} is given by structural beam properties such as the cross section shape and the link length. A graphical representation of this equation is given in Fig. 2(b) where an equivalent torsional spring with stiffness k_{eq} determines the relation between the environment torque τ_e (due to F_e) and the angular displacement $(\theta - q)$.

The second modeling assumption we consider is motivated by the extremely low inertia of certain plastic materials which allows to assume the link as massless. Even if in practice the link inertia is always a finite quantity, its value can be order of magnitude lower with respect to the inertia of a rigid metal link and it is definitely negligible with respect to the reflected inertia of high torque motors which are usually required in human-interaction applications. In this case (when $J_l \ll J_m$) the system behavior is qualitatively different (from the case $J_l \sim J_m$) and it is our opinion that structurally different models can better explain this diversity. From our experimental tests, the massless link model in Fig. 1(b) is the simplest model able to explain the behavior of SELs. Using the massless link model we infer some properties of the SEL closed loop system (in Section III) and we validate them experimentally (in Section V), thus proving coherence between our modeling assumptions and experiments. We highlight that the massless link assumption may be considered with caution in robotic applications where an inertial body needs to be arranged on the link (e.g., the next motor and the next link in a serial kinematics robot). Beside exoskeletons and single joint orthoses, the assumption holds in applications where the link is placed distally and is in direct contact with the human or the environment. An example can be a 2-DOF system with an elastic link attached to a spherical joint. Other examples are represented by parallel robots where motors are typically arranged on the base and each link is in contact with the load or the environment.

As a conclusion, the following points summarize the discussed modeling choices and assumptions:

- Fig. 1(b) can be considered a realistic model for SEA, where the spring represents a real spring arranged between the motor and the link.
- Fig. 1(a) can be assumed as a realistic model for SEL, where the spring represents the whole link and is characterized by an equivalent stiffness $k = k_{eq}$ which is due to the link bending stiffness and negligible inertia.

III. SERIES ELASTIC LINK PROPERTIES

This Section formally states some advantages of SELs with respect to SEAs in single-DOF applications and motivates why SELs retain the same force controllability of SEAs. In particular, we show that the link deformation provides a more *direct measure* of the robot-environment interaction force and that, given the low inertia of plastic materials, transparency and impact-safety can be significantly improved. The following propositions refer to the case of SEL (modeled by (1)–(2) as in Fig. 1(a)) in comparison to the case of SEA (modeled by (3)–(4) as in Fig. 1(b)) when driven by the same motor with inertia J_m .

Proposition 1: Let us consider the SEL model (1)–(2), then the link deflection measures the true robot-environment interaction force τ_e .

The validity of this proposition is a simple consequence of our modeling assumptions. Indeed, model (1)–(2) states that the link deflection is proportional to the torque τ_s which in turn is equal to τ_e . The same statement is not true in the case of the SEAs because the spring torque τ_s is different from the interaction torque τ_e because of the in-between link dynamics, as described by equation (4).

Proposition 2: In the case of collision with a stiff environment, the SEL model (1)–(2) shows enhanced impact tolerance with respect to the SEA model (3)–(4) when driven by the same motor with inertia J_m .

Let us assume that the inertial blocks in Figs. 1(a) and 1(b) are completely rigid and let us consider an environment in the form of a rigid kinematic constraint. When the robot link is approaching such environment with a constant velocity \dot{q}_0 , by virtue of momentum conservation, it turns out that in the case of SEL (Fig. 1(a)) the impact force is a finite quantity whereas in the case of SEA (Fig. 1(b)) the impact force $F(t)$ is theoretically impulsive.¹ This holds both in the cases of elastic and inelastic collisions and proves Proposition 2.

A desired characteristic in robots that interact with humans is transparency. Transparency can be defined as the ability to display a low output impedance in zero mode force control (i.e., when using zero as force reference). Unfortunately, in the case of SEAs such output impedance is dominated by the link inertia which cannot be masked using force control and can be considerably high. Formally, one can consider a simple

¹Theoretically, a collision implies an abrupt change (a discontinuity) in velocity which in the case of an inertial body (e.g., the SEA link) needs an impulsive force. Differently, a purely elastic body (e.g., the SEL link) can be subject to velocity discontinuities without needing impulsive (or infinite) forces.

proportional control law such as

$$\tau_m = -P(\tau_s - \tau_{ref}) \quad (7)$$

where P is a proportional force control gain and the force reference τ_{ref} is set to zero. Substituting this control law in the SEA model (3)–(4) the following closed-loop dynamics can be computed

$$\frac{J_m}{P+1} \ddot{\theta} = -\tau_s \quad (8)$$

$$J_l \ddot{q} = \tau_s - \tau_e \quad (9)$$

where the motor inertia is reduced by a factor $P+1$ while the link inertia J_l is not. This is because the force sensor in SEAs is located before the link, i.e., between the motor and the link. Differently, the force sensor in SELs is the link itself which theoretically allows to mask the (even low) link inertia.

The remaining part of this section expands on the fact that, beside the above mentioned advantages, the SEL architecture retains the same force controllability of SEAs. Leveraging on the considerations in Section II where we showed that a SEL can be modeled as a SEA with negligible link inertia, force control robustness of SELs can be motivated using the same argumentations reported for SEAs, which have been often based on the ideal SEA model in Fig. 1 a. Robinson observed that the actuator stiffness is on the same path of force feedback, thus by decreasing the actuator stiffness it is possible to increase the force control gains without altering stability margins [7]. This leads to improve transparency and to dominate non linear motor dynamics such as stiction, backlash and cogging torques [7], [19]. A similar finding was anticipated by Whitney who proved that interacting with a soft environment improves the force stability margins [20]. Even if the analysis by Whitney, was originally conceived for the case of rigid robots driven by hydraulic actuators, it can be extended to the case of soft robots driven by electromagnetic motors. This extension is reported in Appendix and shows that, differently from rigid robots, series compliance allows unconditional force control stability in spite of environment uncertainties. As they are modeled similarly, this result holds for both SEA and SEL architectures, see the Appendix for details.

IV. SERIES ELASTIC LINK IMPLEMENTATION

In this letter the SEL architecture is implemented using a plastic hollow tube with an outer diameter $D = 20$ mm, and inner diameter $d = 19$ mm and a length of $L = 350$ mm. The tube material is polyvinyl chloride which is characterized by a Young's modulus of about 3 GPa. According to equation (6) and considering that, in the case of a hollow tube the area moment of inertia can be computed as $I = \pi(R^4 - r^4)/4$, this leads to an equivalent torsional² stiffness k_{eq} in the range of 100 Nm/rad which is sufficiently high to support a lightweight robot structure and sufficiently low to ensure good force controllability. Indeed,

²As explained in Section II the torsional stiffness k_{eq} is an equivalent representation for the link bending stiffness (see Fig. 2) and should not be confused with the torsional stiffness of the plastic tube.

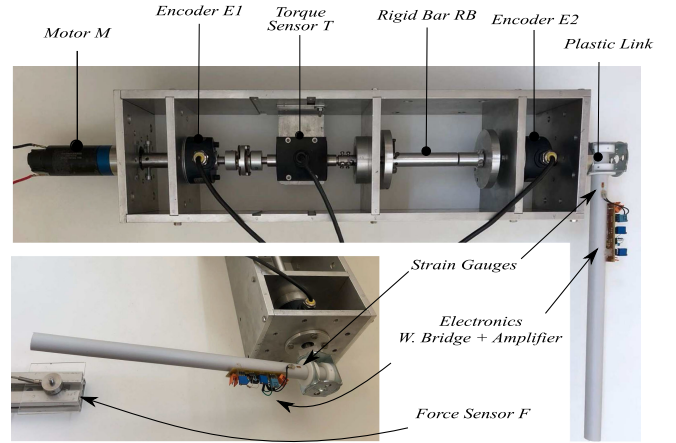


Fig. 3. The modular mechanical setup in SEL configuration.

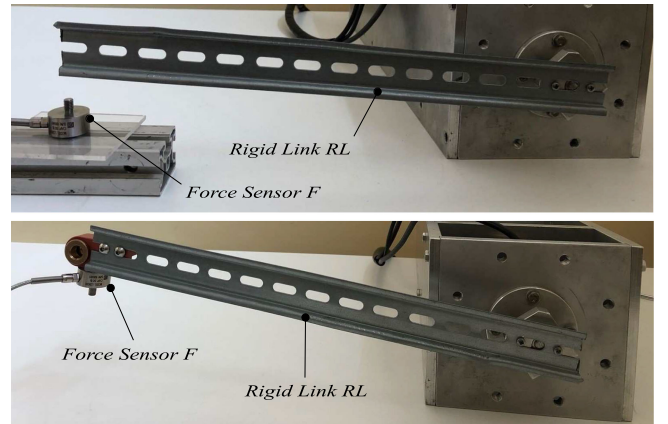


Fig. 4. SEA configuration using a lightweight rigid link. The force sensor F can be arranged on the environment (upper picture) or on the link (lower picture).

this stiffness value is comparable to common choices reported in the literature for SEA-driven human-interacting robots [10], [21]–[24]. In our preliminary prototype, the link deformation is sensed locally using a couple of strain gauges arranged as in Fig. 3. However, different deformation sensing methods can be conceived which may even span the entire link. The strain gauges are connected to a custom electronic board which includes a Wheatstone bridge, an amplification stage and a filtering stage with cut-off frequency at 1.5 kHz. The instrumented plastic link has been mounted on a modular mechanical setup as represented in Fig. 3. The setup includes a geared motor M , a commercial torque sensor T (model AEP RT2A) which is used only for identification purposes, and a commercial force sensor F (model Futek LCM300) used to measure the interaction forces with the environment. The setup can be arranged in both SEL and SEA configurations. In the SEL configuration the encoders E_1 and E_2 are connected using a rigid bar RB and both measure the angle θ described in model (1). In the SEA configuration the rigid bar RB is substituted by a spring S (characterized by a torsional stiffness $k = 78$ Nm/rad) and the plastic link is substituted by a rigid link RL . To provide conservative experimental results we considered an extremely lightweight rigid link, built using a commercial DIN bar as shown in Fig. 4. Depending

TABLE I
 PARAMETERS

System Parameters	
Motor and drive-train inertia	$J_m = 20.6 \cdot 10^{-3} \text{ kg} \cdot \text{m}^2$
Drive-train inertia	$J_{DT} = 0.26 \cdot 10^{-3} \text{ kg} \cdot \text{m}^2$
Rigid Link Inertia (<i>RL</i>)	$J_{RL} = 4.4 \cdot 10^{-3} \text{ kg} \cdot \text{m}^2$
<i>RL</i> with force sensor support	$J_{RLFS} = 10.6 \cdot 10^{-3} \text{ kg} \cdot \text{m}^2$
Plastic Link Inertia	$J_{PL} = 0.295 \cdot 10^{-3} \text{ kg} \cdot \text{m}^2$
SEL stiffness	$k_{eq} = 102 \text{ Nm/rad}$
SEA stiffness	$k = 78 \text{ Nm/rad}$
Control Tuning	
Proportional Gain	$P = 4$
Derivative Gain	$D = 8$

on the configuration and on the specific experiment, the sensor F is arranged on the rigid link, on the plastic link or on the environment. System parameters have been estimated using a procedure similar to the one described in [25] and are reported in Table I.

Force control is implemented using a proportional-derivative (PD) control law in the form

$$\tau_m = -P(\tau_s - \tau_{ref}) - D\dot{\tau}_s \quad (10)$$

considering the same tuning for both the SEA and SEL configurations, see Table I. The control process runs on a standard PC at 3 kHz and communicates with the motor drive and the sensor electronics via Ethercat protocol at the same rate. Controllers are implemented in C++ within the Series Elastic Library architecture (<http://metropolis.scienze.univr.it/altair/selib/>).

V. EXPERIMENTAL VALIDATION

Three experiments are designed to experimentally validate the statements in Section III. In the case of SEA the feedback torque is computed as $\tau_s = k(\theta - q)$ using encoders $E1$ and $E2$ to measure θ and q while the case of SEL the link deformation is measured locally using strain gauges. The additional force sensor F is used to measure the interaction torque τ_e and is arranged on the environment (during experiments 1 and 2) or on the link (during experiment 3).

A. Experiment 1

The objective of the first experiment is to measure the force tracking performance of SEL and SEA arrangements when interacting with a rigid environment. In this experiment the link (either plastic or rigid) is placed in contact with a stiff environment and a discontinuous force reference is commanded to push against it. Control responses are reported in Fig. 5 where τ_{ref} represents the desired torque, τ_s is the torque measured by spring compression (in SEA) or link deformation (in SEL) and τ_e is the true interaction force with the environment measured using the force sensor F arranged on the environment. A fast and accurate step response is observed for both the configurations; in the case of SEL we measured a rise time of about 10 ms

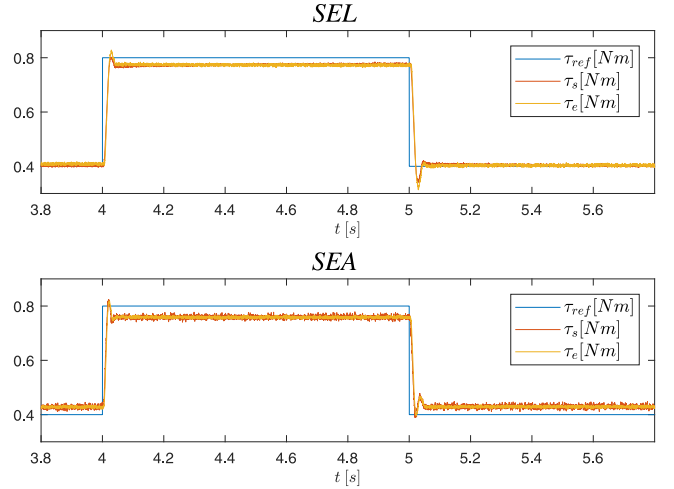


Fig. 5. Torque tracking experiments using SEL and SEA configurations. τ_{ref} is the torque reference, τ_e is the interaction force with the environment measured the force sensor F and τ_s is the torque measured by link deformation (in SEL) or spring compression (in SEAs).

and a maximum static error of 3.5%. A similar response is observed for the SEA configuration (rise time: 9 ms, static error: 5.0%). The similar characteristics of SEL and SEA responses confirm our theoretical expectations. Finally, we observe that, as the experiment only involves static conditions, the torques estimated by spring or link deformation (τ_s , in red) are always close to the ones measured by the commercial sensor F (τ_e , in yellow).

B. Experiment 2

This experiment is designed to show the impact responses of SEL and SEA architectures. An impedance controller is implemented using an inner PD force loop tuned with $P = 2$, $D = 0$ and an outer position feedback

$$\tau_{ref} = -k_{des}(q - q_{ref}) + g(q), \quad (11)$$

where k_{des} is the desired stiffness, q_{ref} represents the impedance equilibrium position (the position when no force is applied), τ_{ref} is the torque reference for the inner force controller and $g(q)$ is a gravity compensation term. The reader is referred to [2], [26], [27] for details on this impedance control implementation. The impedance stiffness is set to $k_{des} = 2 \text{ Nm/rad}$ and the equilibrium position q_{ref} is commanded with a sinusoidal signal causing impacts on a metal surface. Results are reported in Fig. 6 which shows the interaction forces with the environment (τ_e , red line) measured by the commercial sensor F (arranged on the environment) and by link or spring deflection (τ_s , yellow line). SEL impact forces are significantly lower in magnitude than those occurred with SEAs. These results confirm the statement in Proposition 2. Moreover, it can be observed that in the case of SEL the torque τ_s is very close to the one measured by the commercial sensor meaning that the link deflection provides an accurate measure of interaction forces, as stated in Proposition 1. Differently, in the case DFSEA configuration, the spring torque τ_s is sometimes far from the interaction torque τ_e as shown in magnification plots. This is because in

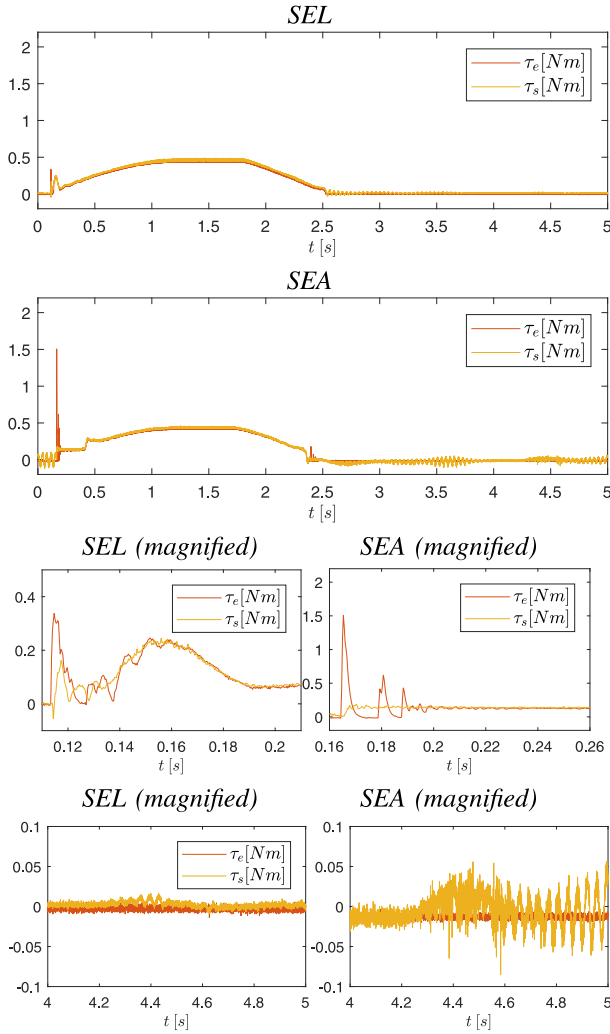


Fig. 6. Impact forces in SEL and SEA during impedance control experiments where the robot link hits a metal surface. τ_s is the torque measured by link deformation (in SEL) or spring compression (in SEA) while τ_e is the interaction force with the environment measured using a commercial force sensor.

dynamical conditions the torque τ_s cannot distinguish between the environment interaction force and the inertial force due to the link. Finally, we observe that SEL impact responses present bumps and contact discontinuities which disappear in the case of SEA. Indeed, the inherent damping of plastic materials may help to dissipate the impact energy and the low weight of plastic links allows to be more easily damped by the control system, when the contact is lost.

C. Experiment 3

This experiment is designed to measure the force control transparency of our SEL and SEA implementations. The PD force controller (10) is set up with zero force as reference and we recorded data from manual perturbations acting on the force sensor F arranged on the link as in Fig. 4, lower picture. The recorded data is used to estimate the apparent robot inertia J_a considering a purely inertial model

$$-\tau_e(t) = J_a \ddot{q}(t) \quad (12)$$

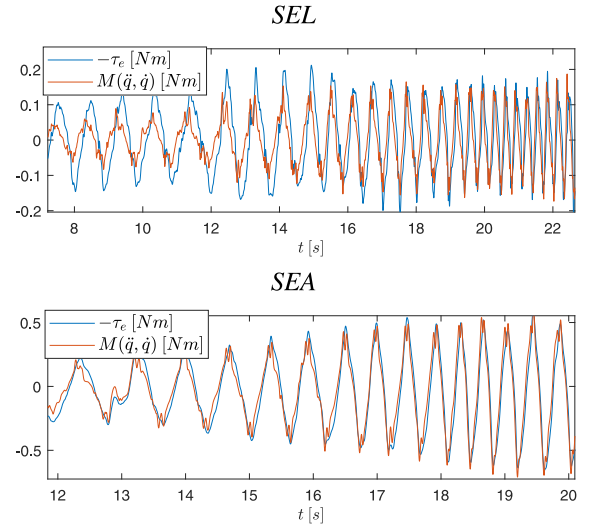


Fig. 7. Identification experiments in zero mode force control under manual perturbations. The plots show that the interaction dynamics can be explained using a purely inertial model.

where $\ddot{q}(t)$ is the recorded acceleration and $\tau_e(t)$ is due to the manual perturbing forces. Fig. 7 reports the related data fitting showing that model (12) can adequately explain the apparent system dynamics. In our testbed, the estimated apparent inertia of the SEL configuration is $J_a = 4.13 \cdot 10^{-3} \text{ kg} \cdot \text{m}^2$ which is extremely close to the value $\frac{J_m + J_{DT}}{P+1} = \frac{20.8 \cdot 10^{-3} \text{ kg} \cdot \text{m}^2}{4+1} = 4.16 \cdot 10^{-3} \text{ kg} \cdot \text{m}^2$ which represents the masked motor inertia only. This agrees with our assumption of negligible link inertia: only the masked motor inertia seems to be perceived. In the case of SEA the apparent inertia is estimated as $J_a = 14.4 \cdot 10^{-3} \text{ kg} \cdot \text{m}^2$ which seems very close to $\frac{J_m + J_{DT}}{P+1} + J_{RLFS} = 14.8 \cdot 10^{-3} \text{ kg} \cdot \text{m}^2$, i.e., the sum of motor and link inertia. As expected, a SEA architecture cannot mask the (possibly high) rigid link inertia. We acknowledge that the motor gearbox presents a mechanical play which may lead to slightly underestimate the parameter J_a : during direction changes the motor may be not in contact with the drive-train leading to a lower output impedance.

VI. CONCLUSIONS AND FUTURE WORK

This work introduces the concept of Series Elastic Link where compliance is implemented by the inherent link flexibility leading to affordable and compact compliant design. It reports our efforts to theoretically and experimentally motivate the similarities between SELs and SEAs as well as certain advantages of SELs with respect to more expensive SEAs. Further steps are planned to characterize and control SELs including the identification of dynamical effects which are not accounted here (e.g., link damping and plasticity), different approaches to sense link deformation (in this work the deformation is measured locally but nothing prevents to exploit the whole link deformation) and more advanced force control methods to provide stable, accurate and predictable responses in spite of environment uncertainties (e.g., [28]–[30]). In this regard the small weight of plastic links

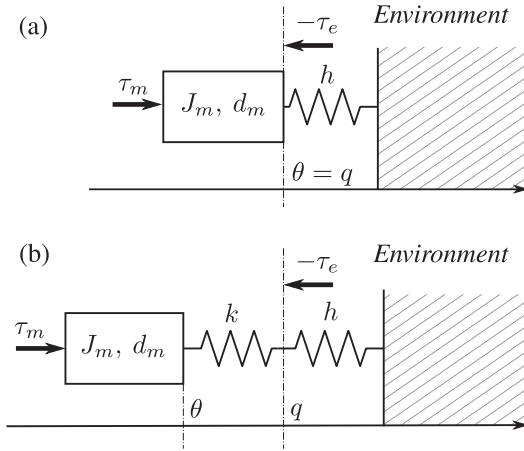


Fig. 8. Plot (a): a rigid robot (modeled as a pure inertia J_m) in contact with the environment (modeled as spring with stiffness h). Plot (b): a compliant robot in contact with the environment where $1/k$ represents the robot series compliance.

can pose some control challenges, especially in the case of extremely soft environments [31].

APPENDIX

In his seminal work Whitney analyzed the stability of a force controlled hydraulic actuator when interacting with an environment modeled as a pure spring [20]. He considered a digital force control implementation in the form

$$\tau_m = -P\tau_e \quad (13)$$

where τ_e measures the interaction force with the environment and P is a proportional gain, and found the following stability condition

$$0 < PT h < 1 \quad (14)$$

where h is the environment stiffness and T is the digital delay. Interestingly, a similar condition can be found by applying the same analysis to the case of an electromagnetic actuator modeled as

$$J_m \ddot{\theta} + d_m \dot{\theta} = \tau_m - \tau_e \quad (15)$$

where θ is the motor position, J_m is the reflected motor inertia, d_m is the viscous coefficient, τ_m is the motor input torque (proportional to the current) and $\tau_e = h\theta$ represents the environment forces, as shown in Fig. 8(b). We observe that model (15) is equivalent to (1) except for the damping term $d_m \dot{\theta}$. By substituting (13) in (15) one can find the following closed loop dynamics

$$[J_m s^2 + d_m s + h(P+1)]\theta = 0 \quad (16)$$

where s is the Laplace variable and by following the methodology proposed by Whitney the continuous-time system can be transformed into the following discrete-time system using the forward Euler method. In Z -transform notation this leads to

$$z^2 + z(\alpha - 2) + (T\alpha\beta - \alpha + 1) = 0 \quad (17)$$

where $\alpha = \frac{d_m T}{J_m}$ and $\beta = h(P+1)$. Finally, stability of the discrete time system (17) is ensured if and only if the roots are within the unitary circle which is equivalent to

$$0 < (P+1)Th < d_m. \quad (18)$$

This condition is similar to (14) and states that environment compliance improves force control robustness: when h decreases the gain and delay margins increase, i.e., P and T can be augmented while retaining the same stability robustness.

Interestingly, condition (18) can be pessimistically interpreted by stating that, given a digital force control implementation with proportional gain P and delay T , it is always possible to find a stiff enough environment to bring the system to instability. This explains why force control of stiff robots has been historically considered a challenging task [32]. Fortunately, when series compliance is introduced, force control becomes unconditionally stable. This can be shown by further extending the analysis by Whitney to the case of the compliant robot driven by electromagnetic actuators, as represented in Fig. 8(b).

Proposition 3: Given the compliant robot model represented in Fig. 8(b) and modeled as (15) where $\tau_e = k(\theta - q) = h\theta$, a digital force control implementation with proportional gain $P < \frac{d_m}{kT}$ is always stable, independently of the environmental stiffness h .

Proof: The proposition can be proved by substituting the environment stiffness h in (18) with the series of robot and environment stiffness $\frac{kh}{k+h}$. Then, the new stability condition becomes

$$0 < PkT < d_m \left(1 + \frac{k}{h}\right) \quad (19)$$

where $1/k$ represents the robot series compliance. Then, by considering the worst case scenario $h \rightarrow \infty$, one can find that a digital force control implementation with positive proportional gain

$$P < \frac{d_m}{kT} \quad (20)$$

is always stable, independently of the environment stiffness h . ■

This extension to the Whitney condition holds whenever a compliant robot can be modeled as in Fig. 8(b) which represents a quite realistic model for SEL. A similar analysis has been reported in our previous work [33] where, however, condition (14) was not extended to the case of electromagnetic actuators.

REFERENCES

- [1] J. D. Schutter, H. Bruyninckx, W.-H. Zhu, and W. Mark, "Force control: A bird's eye view," in *Lecture Notes in Control and Information Sciences*, vol. 230. Berlin, Germany: Springer, 1998, pp. 1–17.
- [2] A. Calanca, R. Muradore, and P. Fiorini, "A review of algorithms for compliant control of stiff and fixed compliance robots," *IEEE Trans. Mechatronics*, vol. 21, no. 2, pp. 613–624, Apr. 2016.
- [3] S. Casey, "Ekso bionics: Ekso (eLEGS)," in *Proc. BME 1st Presentation*, 2014, p. 2014.
- [4] T. Nef, M. Mihelj, G. Kiefer, C. Perndl, R. Muller, and R. Riener, "ARMin-exoskeleton for arm therapy in stroke patients," in *Proc. 10th IEEE Int. Conf. Rehabil. Robot.*, 2007, pp. 68–74.
- [5] G. Colombo and M. Morari, "Rehabilitation with a 4-DOF robotic orthosis," *IEEE Trans. Robot.*, vol. 20, no. 3, pp. 574–582, 2004.

- [6] G. A. Pratt and M. Williamson, "Series elastic actuators," in *Proc. IEEE Int. Conf. Intell. Robots Syst.*, 1995, vol. 1, pp. 399–406. [Online]. Available: http://ieeexplore.ieee.org/xpls/abs_all.jsp?arnumber=525827
- [7] D. W. Robinson, "Design and analysis of series elasticity in closed-loop actuator force control," Ph.D. dissertation, Dept. Mech. Eng., Massachusetts Inst. Technol., Cambridge, MA, USA, 2000.
- [8] M. Williamson, "Series elastic actuators," Dept. Mech. Eng., Ph.D. dissertation, Massachusetts Inst. Technol., Cambridge, MA, USA, 1995.
- [9] N. Georgiev and J. Burdick, "Design and analysis of planar rotary springs," no. II, pp. 4777–4784, 2017.
- [10] F. Giovacchini *et al.*, "A light-weight active orthosis for hip movement assistance," *Robot. Auton. Syst.*, vol. 73, pp. 123–134, Sep. 2014. [Online]. Available: <http://linkinghub.elsevier.com/retrieve/pii/S0921889014001730>
- [11] R. H. Cannon and D. E. Rosenthal, "Experiments in control of flexible structures with noncollocated sensors and actuators," *J. Guid. Control*, vol. 3, no. 3, pp. 546–553, 1984.
- [12] M. Benosman and G. Le Vey, "Control of flexible manipulators: A survey," *Robotica*, vol. 22, no. 5, pp. 533–545, 2004.
- [13] J. Malzahn and T. Bertram, "Collision detection and reaction for a multi-elastic-link robot arm," *IFAC Proc. Vol. (IFAC-PapersOnline)*, vol. 19, pp. 320–325, 2014.
- [14] J. Malzahn, R. F. Reinhart, and T. Bertram, "Dynamics identification of a damped multi elastic link robot arm under gravity," in *Proc. IEEE Int. Conf. Robot. Automat.*, 2014, pp. 2170–2175.
- [15] J. Malzahn, A. S. Phung, F. Hoffmann, and T. Bertram, "Vibration control of a multi-flexible-link robot arm under gravity," in *Proc. IEEE Int. Conf. Robot. Biomimetics*, 2011, pp. 1249–1254.
- [16] J. Malzahn, R. Schloss, and T. Bertram, "Link elasticity exploited for payload estimation and force control," in *Proc. IEEE Int. Conf. Intell. Robots Syst.*, 2015, pp. 1508–1513.
- [17] A. Garcia and V. Feliu, "Force control of a single-link flexible robot based on a collision detection mechanism," *IEE Proc. Control Theory Appl.*, vol. 147, no. 6, pp. 588–595, 2000. [Online]. Available: http://digital-library.theiet.org/content/journals/10.1049/ip-cta_20000524
- [18] Y. Morita, F. Matsuno, Y. Kobayashi, M. Ikeda, H. Ukai, and H. Kando, "Dynamics based force control of a one-link flexible arm considering bending and torsional deformation," *Trans. Soc. Instrum. Control Eng.*, vol. 38, no. 6, pp. 549–556, 2002. [Online]. Available: https://www.jstage.jst.go.jp/article/sicetr1965/38/6/38_6_549/article
- [19] R. D. Howard, "Joint and actuator design for enhanced stability in robotic force control," Ph.D. dissertation, Dept. Mech. Eng., Massachusetts Inst. Technology, Cambridge, MA, USA, 1990.
- [20] D. Whitney, "Force feedback control of manipulator fine motions," *Trans. ASME J. Dyn. Syst. Meas. Control*, vol. 99, no. 2, pp. 91–97, 1977.
- [21] W. Roozing, J. Malzahn, N. Kashiri, D. G. Caldwell, and N. G. Tsagarakis, "On the stiffness selection for torque-controlled series-elastic actuators," *IEEE Robot. Lett.*, vol. 2, no. 4, pp. 2255–2262, Oct. 2017.
- [22] Rethink Robotics, "Baxter Research Robot—Hardware Specifications," 2015. [Online]. Available: http://sdk.rethinkrobotics.com/wiki/Hardware_Specifications
- [23] G. Carpino, D. Accoto, F. Sergi, N. Luigi Tagliamonte, and E. Guglielmelli, "A novel compact torsional spring for series elastic actuators for assistive wearable robots," *J. Mech. Des.*, vol. 134, no. 12, 2012, Art. no. 121002. [Online]. Available: <http://mechanicaldesign.asmedigitalcollection.asme.org/article.aspx?doi=10.1115/1.4007695>
- [24] F. Sergi, D. Accoto, G. Carpino, N. L. Tagliamonte, and E. Guglielmelli, "Design and characterization of a compact rotary series elastic actuator for knee assistance during overground walking," in *Proc. IEEE RAS EMBS Int. Conf. Biomed. Robot. Biomechatronics*, 2012, pp. 1931–1936.
- [25] A. Calanca, L. M. Capisani, A. Ferrara, and L. Magnani, "MIMO closed loop identification of an industrial robot," *IEEE Trans. Control Syst. Technol.*, vol. 19, no. 5, pp. 1214–1224, Sep. 2011. [Online]. Available: http://ieeexplore.ieee.org/xpls/abs_all.jsp?arnumber=5634145http://ieeexplore.ieee.org/lpdocs/epic03/wrapper.htm?arnumber=5634145
- [26] A. Calanca and P. Fiorini, "Impedance control of series elastic actuators: Passivity and acceleration-based control," *Mechatronics*, vol. 47, pp. 37–48, 2017. [Online]. Available: <http://linkinghub.elsevier.com/retrieve/pii/S0921889016303256>
- [27] N. L. Tagliamonte and D. Accoto, "Passivity constraints for the impedance control of series elastic actuators," *J. Syst. Control Eng.*, vol. 228, no. 3, pp. 138–153, 2013.
- [28] A. Calanca and P. Fiorini, "Human-adaptive control of series elastic actuators," *Robotica*, vol. 2, no. 8, pp. 1301–1316, 2014.
- [29] A. Calanca and P. Fiorini, "Understanding environment-adaptive force control of series elastic actuators," *IEEE/ASME Trans. Mechatronics*, vol. 23, no. 1, pp. 413–423, Feb. 2018.
- [30] A. Calanca and P. Fiorini, "Impedance control of series elastic actuators based on well-defined force dynamics," *Robot. Auton. Syst.*, vol. 96, pp. 81–92, 2017. [Online]. Available: <http://dx.doi.org/10.1016/j.robot.2017.06.013>
- [31] A. Calanca and P. Fiorini, "A rationale for acceleration feedback in force control of series elastic actuators," *IEEE Trans. Robot.*, vol. 34, no. 1, pp. 48–61, Feb. 2018.
- [32] S. Eppinger and W. Seering, "Understanding bandwidth limitations in robot force control," in *Proc. IEEE Int. Conf. Robot. Automat.*, 1987, vol. 4, pp. 904–909. [Online]. Available: http://ieeexplore.ieee.org/xpls/abs_all.jsp?arnumber=1087932
- [33] A. Calanca and P. Fiorini, "On the role of compliance in force control," in *Advances in Intelligent Systems and Computing*, E. Menegatti, N. Michael, K. Berns, and H. Yamaguchi, Eds., vol. 302. Padova, Italy: Springer, 2016, pp. 1243–1255.